Surface Heating from Remote Sensing of the Hypervelocity Entry of the NASA GENESIS Sample Return Capsule

Peter Jenniskens*
SETI Institute, 515 N. Whisman Rd., Mountain View, CA 94043 (pjenniskens@mail.arc.nasa.gov)

Paul F. Wercinski†, Joseph Olejniczak, Michael Wright, George Raiche, and Dean Kontinos
NASA Ames Research Center, Moffett Field, CA 94045

Prasun N. Desai
NASA Langley Research Center, Hampton VA

Richard E. Spalding and Kurt Sandquist
Sandia National Laboratory, Albuquerque, NM

George Rossano and Ray W. Russell
The Aerospace Corporation, 2350 E. El Segundo Bl., El Segundo, CA 90245-4691

Douglas O. Revelle
Los Alamos National Laboratory, Los Alamos, NM

and

Donald Hladiuk and Alan R. Hildebrand
Meteorites and Impact Advisory Committee, University of Calgary, Calgary, Canada

An instrumented aircraft and ground-based observing campaign was mounted to measure the radiation from the hypervelocity (11.0 km/s) reentry of the Genesis Sample Return Capsule prior to landing on the Utah Test and Training Range on September 08, 2004. The goal was to validate predictions of surface heating, the physical conditions in the shock layer, and the amount and nature of gaseous and solid ablation products as a function of altitude. This was the first hypervelocity reentry of a NASA spacecraft since the Apollo era. Estimates of anticipated emissions were made. Erroneous pointing instructions prevented us from acquiring spectroscopic data, but staring instruments measured broadband photometric and acoustic information. A surface-averaged brightness temperature was derived as a function of altitude. From this, we conclude that the observed optical emissions were consistent with most of the emitted light originating from a gray body continuum, but with a surface averaged temperature of 570 K less than our estimate from the predicted heat flux. Also, the surface remained warm longer than expected. We surmise that this is on account of conduction into the heat shield material, ablative cooling, and finite-rate wall catalycity. Preparations are underway to observe a second hypervelocity reentry (12.8 km/s) when the Stardust Sample Return Capsule returns to land at U.T.T.R. on January 15, 2006.

Nomenclature

A = projected surface area (in m^2)
$B_\lambda (T)$ = Planck curve

* Mission Scientist, SETI Institute, no AIAA member
† Program manager, NASA Ames Research Center, AIAA Member Associate Fellow

c = speed of light = 2.99793 x 10^8 m/s
C_d = drag coefficient
D = the distance to the SRC (in m)
h = Planck constant = 6.62620 x 10^{-34} J s
k = Boltzmann's constant = 1.38062 x 10^{-23} J/K
λ = wavelength (m)
MAC = Multi-Instrument Aircraft Campaign
ρ = air density
SRC = Sample Return Capsule
T = temperature

Introduction

THE Genesis Sample-Return-Capsule (SRC) Entry Observing campaign ("Hyperseed MAC") aimed to deploy spectrographic, imaging, and infrasound instruments to derive the physical conditions during reentry of the Genesis Sample-Return-Capsule.[1] These data can be used for the evaluation of aerothermal heating and material response models,[2] shock layer radiation models, Thermal Protection System (TPS) performance, accident investigations, and for studies of the delivery of organic compounds for the origin of life by small-asteroid impacts.[3] This particular entry was significant because it was the first hypervelocity reentry from interplanetary space since the Apollo era. In general, a validation of the heating conditions of hypervelocity entries can justify the future engineering of thermal protection systems of lesser weight.

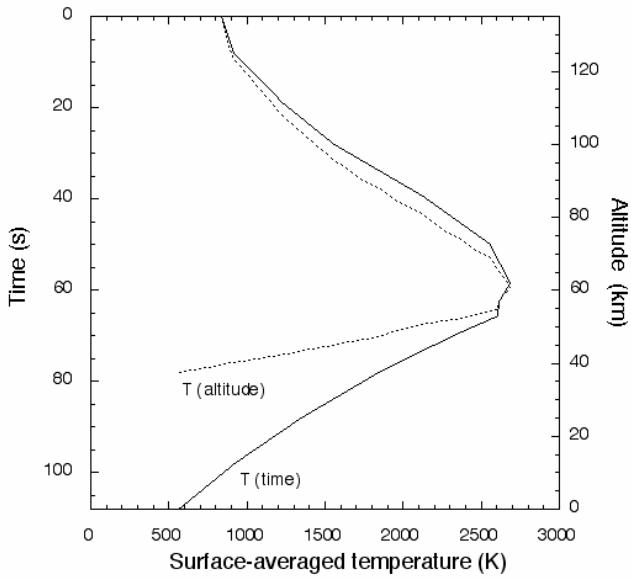

Figure 1. Predicted surface temperature, *as a function of both capsule altitude (dotted line) and time since passing the 135 km altitude point (solid line), derived from the integrated emission over the whole surface area, assuming a radiative equilibrium wall and no shock emission.*

The surface of the Genesis SRC is a 1.5 inch thermally-conductive high-density (1.8 g/cm^3) high-temperature (2,870 K) deposited carbon-carbon sheet (made of fibers of highly ordered pyrolytic carbon) on top of a low-density carbon foam insulator. The capsule has a surface area of only 1.81 m^2, so small that the remote-sensing observations discussed here make this an unresolved point source.

The entry speed was 11.0 km/s at 135 km altitude, with an attack angle of 8º, and a spin rate of 15/s. Radiative heat flux becomes important relative to convective heat flux for speeds in excess of V > 11 km/s. In the case of Genesis, about 5% of the heat flux is expected to be due to radiative heat flux.

The actual conditions of descent have never been simulated in the laboratory for all relevant parameters at the same time. The NASA/Ames Arcjet Facility mimics the convective heat flow well (albeit with pre-dissociated air), while shock-tube experiments provide good measurements of the radiative heat flux (albeit for a brief moment of time).

Expected emissions

In preparation of an instrumented airborne and ground-based observing campaign, we examined the expected flow field environment and radiation signatures from the shock wave and from the reentry body surface and ablation products, based on the projected trajectory version REF-08. The predictions are elaborated on elsewhere.[4] Here, we summarize the points relevant to the interpretation of the observations.

1. Blackbody radiation.

The anticipated optical signature was a combination of the gray body emission from the capsule surface and the atomic, molecular, bound-free, and free-free emission from the shock layer. The relative intensities of the surface emission and shock layer emission depend on both the altitude (time along the trajectory) and the wavelength region being considered. Figure 1 shows the anticipated change in surface temperature based on fully catalytic radiative equilibrium computational fluid dynamics (CDF) calculations. The blackbody radiance from the hot SRC surface varies with the fourth power of surface temperature, and surface-averaged temperatures can be derived accurately from the intensity of the continuum emission.

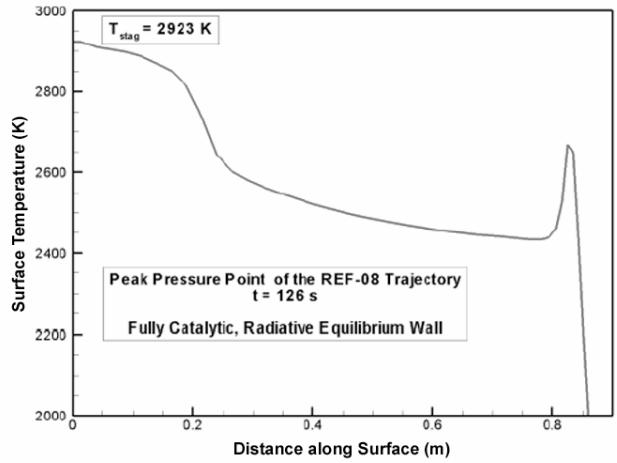

Figure 2. Plot of the radial distribution of the Genesis SRC surface temperatures. *A peak temperature of 2923 K is found at time = 126 s for the REF-08 Genesis descent trajectory. A fully catalytic, radiative equilibrium wall is assumed.*

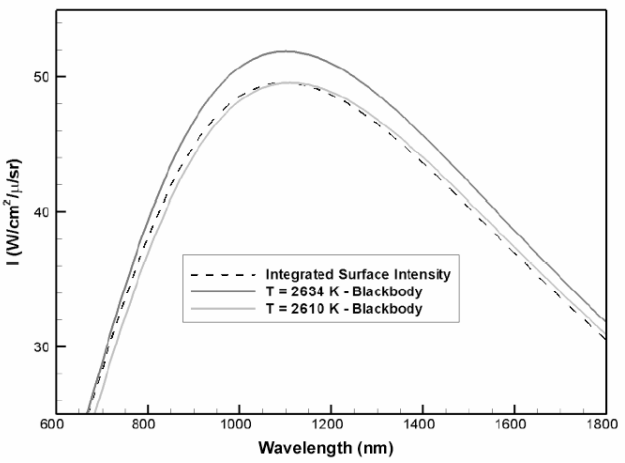

Figure 3. Integrated surface intensity (dashed line) compared to single-temperature blackbody emissions at 2634 and 2610 K.

The distribution of surface temperatures has an impact on the expected wavelength dependent signal. Surface temperatures will range from about 2,400 to 2,923 K (Figure 2), causing light emission to peak near 1 micron. Figure 2 shows the surface temperature distribution along a radial line originating at the stagnation point at the center of the spherical section. The maximum surface temperature occurs at the stagnation point.

There are additional hot spots at the forebody penetration points that are not modeled. These penetration regions are only a small fraction of the total are and are not expected to produce a strong deviation from a blackbody shape.

Since the area of the stagnation region is small compared to the conical flank, we expect that the observed total emission will be characterized by the intermediate temperatures off the stagnation line of around 2,600 K. An "Integrated Surface Intensity" is calculated by adding the area-weighted contributions of intensity from each surface point (Fig. 1). The resulting wavelength-dependent curve deviates slightly from a Planck curve (Figure 3). The integrated distribution has a lower peak than the T = 2,923 K curve. The integrated distribution would suggest a temperature of T ~ 2,634 K at short wavelengths near 700 nm, but T ~ 2,610 K at longer wavelengths near 1600 nm. These differences may be sufficient to retrieve information about the surface temperature distribution from remote sensing observations.

Line-of-sight variations in intensity when the Sample Return Capsule passes by the observer and the viewing angle changes from near head-on to side views, can also be used to evaluate the distribution of temperature on the surface, if the orientation of the capsule and viewing angle are known.

2. Shock radiation.

At high enough spectral resolution, shock emission from nitrogen and oxygen atoms, the first negative system of N_2^+, and the first positive band of N_2, are predicted to stand out above the blackbody, bound-free, and free-free continuum. This radiation produced in the high temperature region immediately behind the shock can heat the surface of re-entry vehicles, a process called *radiative heat flux*.

For the Genesis entry, the amount of radiative heating is predicted to be about 30 W/cm^2. For comparison, the convective heating is predicted to be about 700 W/cm^2. For the upcoming faster (12.8 km/s) Stardust SRC entry, the convective heating is predicted to be about 1200 W/cm^2, and the radiative heating about 130 W/cm^2.

This radiation is emitted from excited (higher energy) electronic states of atoms/molecules and atomic/molecular interactions with free electrons. Emission processes are generally well-understood, based on laboratory spectroscopic data and calculations. The rate of produced emission is less certain, because it depends on the excitation conditions and gas density in the shocked layer, as well as the presence of ablation products. Traditional CDF codes compute the number of atoms/molecules in the ground electronic state. An excitation model is needed to calculate number of electronically excited molecules and the distribution of those molecules among vibrational and rotational states based on CFD results. Models that describe the amount of absorption in the shocked layer are needed to compute the transport of photons from the shock region to the surface and the radiative heating at the surface. The theory for such models is well understood, but the necessary absorption coefficient data is lacking.

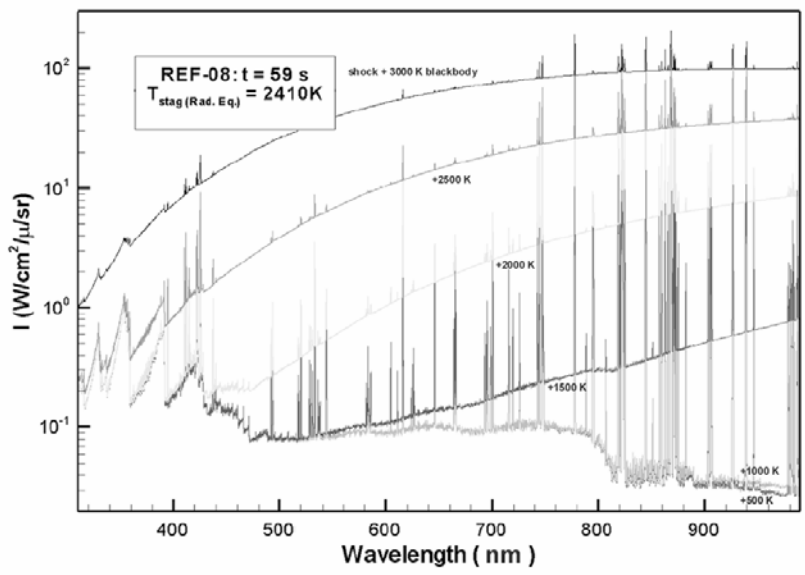

Figure 4. Expected optical emissions from shock radiation, *superimposed on various blackbody radiation levels. An instrumental spectral resolution of 0.3 nm was adopted.*

One of us (J.O.) performed CFD (DPLR) calculations for 11 species air (N_2, O_2, NO, N, O, N_2^+, O_2^+, NO^+, N^+, O^+, e^-) at 7 points on the preliminary Genesis trajectory called "REF-08", which is close to the actual trajectory over the wavelength range $0.3 < \lambda < 1.0$ μm. Shorter wavelength measurements are not possible due to atmospheric absorption. Longer wavelength lines and bands are currently not included and/or verified in NEQAIR. The shock layer emission in the direction of the observing plane is assumed to be optically thin. We also neglect atmospheric absorption between the capsule and the observing plane, which is reasonable. At times prior to t = 40 s, when the capsule is at high altitudes, the SRC may not be in the continuum flow regime and the Navier-Stokes results are suspect.

Figure 4 shows the sum of shock emissions and surface blackbody radiation during peak heating at t = +59 seconds, for a range of adopted surface temperatures. The expected emission at this time would have a spectral dependence similar to that of the second curve from the top. The excitation temperatures in the shock vary, but the primary radiators include the $N_2[1^+]$ band, the $N_2^+[1^-]$ band, and N & O lines. There is also a weak continuum from the electrons in the shock layer. The shock radiation is primarily emitted from the "overshoot" region immediately behind the shock wave. The computed radiative equilibrium stagnation point temperature (T = 2,410 K at this point in time) is an upper bound on the surface temperature. Note that the blackbody curves represent the integrated average surface temperatures expected at different times during descent. The shock layer emission shown represents a volume-averaged value.

If the surface temperature of the SRC rises above about 1700 K, we expect that the blackbody radiation from the surface will dominate the total light output at green, red, and near-IR wavelengths. Blue wavelengths may contain a significant signature from the $N_2^+[1^-]$ band and plasma continuum emissions.

At high enough spectral resolution, we find that band emission below 400 nm and the near-IR atomic lines of oxygen and nitrogen should be discernible even early in the trajectory. A higher spectral resolution will cause the atomic lines to stand out better from the blackbody background. There are significant changes in the excitation conditions along the trajectory and the emission spectrum is expected to change. However, band emission below 400 nm and atomic lines should be discernible even past peak pressure, when both shock emissions and surface emissions are weaker.

3. Emissions from ablation products.

Emission features from ablation product species such as carbon atomic lines, sodium lines (sodium being an impurity in the heat shield material), the CN Violet band, and the mid-IR 4.6 micron CO band may also be detected, providing information about the ablation process. CN and CO are chemical products from the interaction of the ablated carbon with the air plasma.

We did not yet fully consider the effect of surface blowing and ablation products (CN, CO, C, C_2, etc.) in the NEQAIR model. For Genesis, the ablation rate averaged over the surface is only about 0.03 kg/s/m^2 at peak heating. For an area of 1.81 m^2, this gives an ablation rate of about 0.05 kg/s for the entire surface. The main ablation product is C (mole fraction X=0.3), followed by CO (X=0.2), and CN (X=0.05). The ablation products do not move at the speed of sound, but rather their velocity depends on local connective velocity in the gas and their diffusion velocity. The CN Violet band at 382 nm may be detectable. CN is generated from the interaction of carbon atoms from the surface with the nitrogen in the shock layer. The emission will be more intense for the Stardust reentry, which is expected to ablate significant amounts of carbon in the form of C, C_2, and C_3.[5]

The expected emission in the near-UV spectrum will be dominated by the isoelectronic N_2^+ bands (with a band head at 391.4 nm instead of 388.1 for CN), separated only in high-resolution spectroscopy.

The near-IR spectrum may include emissions of OH (Meinel) and O_2, and of NO at longer wavelength. Even carbon atom line emissions may be detected during the early parts of the descent of the Stardust SRC, which has a higher rate of ablation. For Genesis, we did not expect to detect these lines.

The mid-IR will be dominated by C-H, C-C and C-O stretch vibration band emissions and continuum emission from debris. Mid-IR measurements of CO (4.67 micron) emission would not only provide an measure of abundance of ablated compounds, but also the temperature of the emitting molecules from the band shape (expected to be anywhere from ~ 3,500 – 10,000 K).

The expected emissions of hot complex carbon molecules, clusters, flakes, and soot grains < 10 micron in size has peaks at 6.2 and 7.7 micron due to C-C stretch and bend vibrations. Reactions with atmospheric water and hydrogen can result in a C-H emission band at 3.4 micron. Little is known about the expected amounts of these materials, which can be deduced from excess emission in the 6-8 micron range.

4. Other interesting phenomena.

Wake emissions are though to be dominated by NO_2 chemiluminescence in the visible. This is a broadband emission hard to distinguish from continuum. Another interesting phenomenon worth investigating is the possible existence of a photoionization halo generated by the UV radiation in the shock wave.[6] Radio echoes have been detected before from manned space vehicles returning to Earth.[7,8] The strong hypersonic shock wave is expected to generate an infrasound signal on the ground. The Genesis SRC entry can help calibrate the current infrasound sensor networks.

Mission scope and objectives

1. Scope and objectives.

Hyperseeed MAC (Multi-Instrument Aircraft Campaign) was a one-day airborne mission out of Edwards AFB in southern California to Oregon (~ 2 hour flight), where the NKC-135 "FISTA" research aircraft was positioned along the track of the approaching reentry vehicle just outside of UTTR restricted air space. The aircraft was deployed out of Edwards AFB on September 08, 2004, and positioned at latitude = 40^{o} 09.8' N, longitude = 114^{o} 19.9' W, and altitude 39,000 ft, at time = 15:52:36 UT, with a true heading of 241.0 ^{o} degrees azimuth (from north) and true air speed of 430 miles/hr.

The instrumented aircraft campaign was equipped with a redundant range of spectroscopic instruments used before for meteor observations during the four missions of the earlier *Leonid Multi-Instrument Aircraft Campaign*.[9] The daytime sky background was expected to make slit-less spectroscopy difficult, but the high-altitude observations would give us a homogeneous background and little or no water vapor absorption in the line of sight. The spectrometers covered a wide range in wavelength at different spectral resolutions, each focussed on detecting specific compounds in the emitting shock layer or key parts of the blackbody emission.

Onboard instruments that were deployed on the FISTA were in particular the "MIRIS" MId-InfraRed Imaging Spectrograph (3-5.5 micron) of The Aerospace Corporation, a wide field mid-IR imaging camera (3-5 microns) of NASA Ames, a high frame-rate imaging spectrograph (500 f/s) of the University of Alaska, a telescopic optical spectrograph (UC San Francisco), a wide field HDTV imaging spectrograph (NASA Ames), a telescopic HDTV imaging spectrograph (NASA Ames), a 2-channel photometer (Sandia National Laboratories), an Echelle spectrograph with AIMIT tracker and wide field spotting scope with long-wavelength cut-off filter (SETI Institute), two InGaAs cameras for near-IR spectroscopy (Utah State University), a wide field camera with sodium filter (Utah State University), a near-UV slit-less spectrograph (SETI Institute), and a still camera (NASA Ames).

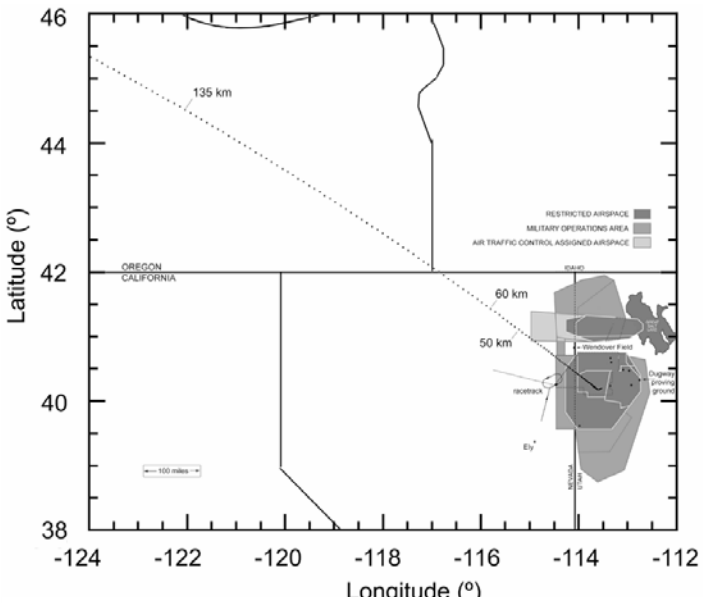

Figure 5. Approach trajectory during descent and position of the FISTA aircraft ("racetrack") just outside the Utah Test and Training Range.

This included imagers with narrow field of view, high frame-rate imagers, and telescopic imagers. The 12" optical windows in the research aircraft diffraction limited the best spatial resolution that might be achieved to about 10 m spatial scale at the distance of the SRC. Hence, potential optical signatures emanating from the forebody penetrations of the Genesis SRC could not be resolved, but larger scale signatures could, such as wake and signatures from UV light absorbed and re-emitted in at optical wavelengths by the ambient environment.

2. Pointing Conditions

Test flights were performed on Friday Sept. 03 and Tuesday Sept. 07, 2004, resulting in much practical experience in the use of slit-less spectrometers under daytime conditions. Spectral responses and field of view were calibrated. Pointing was practiced using Venus as a target. These test flights also served as practice for instrument set-up, data collection logistics, safety and flight operations, and FISTA flight performance and handling qualities. The Air Force flew a very stable platform.

Concern about the potential brightness of the Genesis SRC, coupled to practical experience during test flights (observed gradient of sky brightness), prompted us to use small object acquisition fields of view (5 - 8º). Because we were uncertain of the predicted intensities, all sensors were operated to follow the target along its predicted path until it would become bright enough to be detected.

The SRC was anticipated to be first seen at 135 -100 km altitude (Figure 1), where the object rapidly increases in intensity with increasing surface temperature. The surface reached peak temperature, and the object reached peak absolute brightness, when it would be at about 60 km altitude at +59 seconds after passing the 135 km altitude point. Highest deceleration was expected to occur at ~50 km altitude, about +66 s in flight. The object then entered at a steep angle onto the Utah Test and Training Range (UTTR), in Nevada. The total duration of the observable emission was predicted to be about 60 - 100 s.

At the time of the Genesis entry, all instruments were checked-out and fully operational. Unfortunately, we derived pointing instructions based on a preliminary entry trajectory data track, which were in error by about 9º in azimuth over the full trajectory (with elevations unchanged). As a result, Genesis was just outside the field of view of all spotting scopes during the full track and none of the spectrographs and imagers designed to follow the target were able to acquire the object in the daytime sky. We did, however, obtain broadband photometric measurements of the latter part of the trajectory from staring cameras which, combined with ground-based observations, provides an overview of the change in the surface averaged temperature during descent.

3. The GENESIS Trajectory.

The Genesis SRC passed the altitude of 135.0 km at 15:52:46.416 UT, very close to the 15:52:46.526 UT value in the E - 8 hour trajectory, a trajectory derived from navigational information 8 hours before entry.

Post-flight, for the hypersonic portion of flight, one of us (PD) calculated the best estimated trajectory based on the best NAV at atmospheric interface (which has very small errors) and the latitude and longitude at drogue deployment time obtained from the UTTR radar data (which also should have small errors). Using these two end points, it was calculated what the multiplier on ρ^*C_d needed to be during the hypersonic portion of flight to match these two end conditions. It was found that an 8.06% reduction in ρ^*C_d from the earlier nominal flight trajectory approximation matched the end conditions very well. In our opinion, most of the this 8% is due to a lower atmospheric density (~6%) observed on entry day, and maybe ~2% due to a lower capsule C_d than that predicted from the aero database.

This lower ρ^*C_d means that the entry was slightly down track from the nominal predicted location at drogue deployment. The maximum deceleration obtained is 27.0 Earth g as compared to 27.2 Earth g from the nominal. The 3-sigma variation in the maximum deceleration from the Monte Carlo is +/-1.84 Earth g, so the Genesis entry was very close to nominal (and well within the extremes). The maximum heating rate would also expected to be very close to the nominal predictions.

Results

1. Photometry.

Successful experiments were only those that worked in staring mode (i.e., relatively wide field of view and not aimed to follow the SRC), which included 1) a still camera which recorded exposures in the B, G, and R color bands, 2) the wide field tracking camera of AIMIT, which was a low-light level video camera with I-band filter, and 3) a 3 – 5 micron broadband Mid Wave IR camera. This data was supplemented by 4) a video from a hand-held camcorder operated near Wells, Nv, and a set of three low-light-level cameras operated from a location near Wild Horse Reservoir, Nv, more to the West. The observations at Wild Horse Reservoir (t = 43 to 54 seconds) have been published by Swift and Suggs[10] and have been translated here into surface-average intensities after correction for viewing angle.

All broadband flux measurements were calibrated by comparison to astronomical sources (Moon and Venus) and translated in surface-averaged intensities by scaling to the instantaneous projected surface area (dependent on

viewing angle) and multiplying by the square of the distance to the source (divided by 4π for unit of steradian). The result is summarized in Fig. 6.

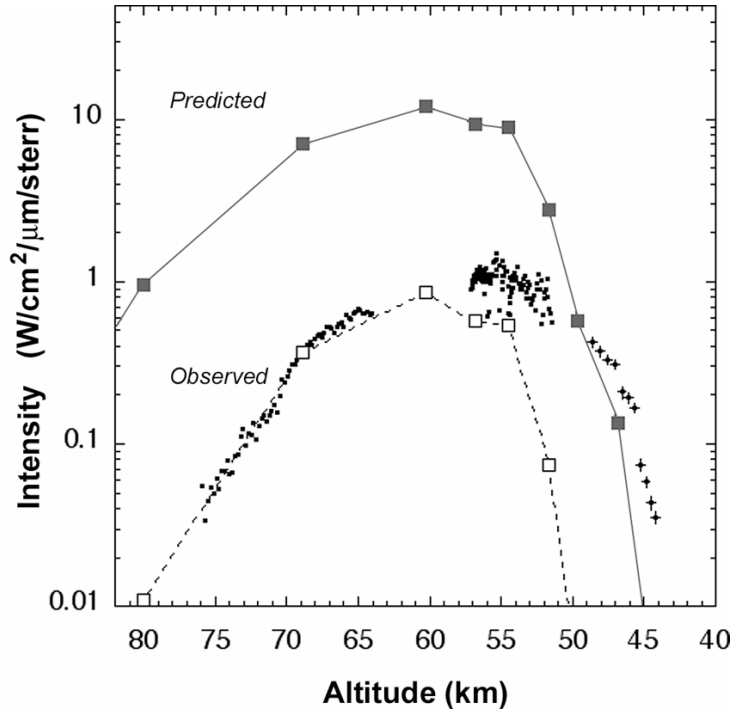

Figure 6. Overview: compilation of surface averaged intensity measurements (•) relevant to the visible wavelength of λ = 548 nm. *Solid squares are predicted intensities derived from the surface temperature (Fig. 1). Open symbols are those predicted intensities scaled down (-570 K) to match the observed intensities.*

The measurements are compared (solid squares) to the expected gray body emission (for emissivity ε = 0.88), derived from the integrated emission over the whole surface area, assuming a radiative equilibrium wall and no shock emission. We confirm the conclusion by Swift and Suggs that the SRC entry was fainter than anticipated, by about a factor of ten (+2.5 magnitudes). The emissivity value is somewhat uncertain (0.76 - 0.93), but that can account for only 10% of the discrepancy. At the onset of the trajectory, the surface was cooler than anticipated by as much as 570±20 K. Open symbols show the predicted values of intensity in case of such systematically lower temperatures. Later in the trajectory, the surface stayed hot longer than expected.

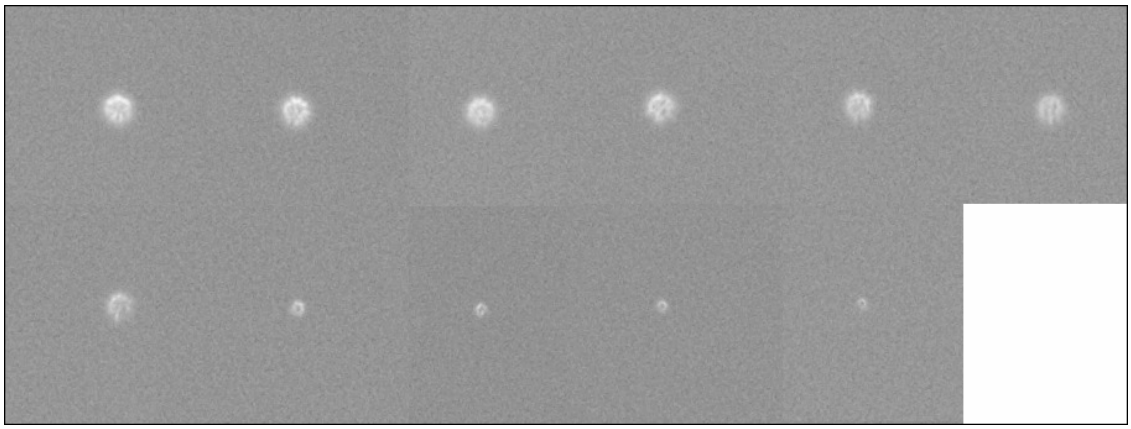

Figure 7. Still images of Genesis SRC. *Change in apparent diameter is due to changing exposure time and focus of the still camera.*

2. Still camera: B, G, and R broadband photometry.

We will now discuss the individual data sets that make up Figure 6. The final part of the trajectory, and the most discrepant with predictions, was covered by a hand held digital still camera (Figure 7). Goal of the hand held still camera photographs was to document large-scale phenomena and measure the optical intensity at the end of the

trajectory, after it left the field of view of other cameras. A Nikon™‡ D70 digital camera was used with a 70-300mm f5.6 Nikon lens. Used hand-held behind a 12" diameter 3/4" thick optical quality BK7 window, set at 400 ASA, with exposure times of 1/1000 - 1/1200s. Eleven exposures were taken, 1 second apart. Time code of the camera's internal clock was calibrated to GPS timing, set by hand to < ±0.3s accuracy. The images are slightly out of focus, spreading the light over many pixels and thus avoiding saturation.

The camera used a SONY™ ICX413AQ CCD detector with image format 3040 x 2014 pixels of size 7.8 microns. We adopted the wavelength response calibration by Christian Bui[11], from which the central wavelength of each band was derived: 460 nm (B-band), 535 nm (V-band), and 600 nm (R-band).

Table I: forebody projected surface area *for different viewing angles (α).*

α °)	projected area (m^2)	total projected area (m^2)
0.0	1.813	1.813
10.0	1.787	1.787
20.0	1.707	1.709
30.0	1.577	1.626
40.0	1.400	1.516
50.0	1.183	1.370
60.0	0.931	1.188
70.0	0.714	1.073
80.0	0.526	1.022
90.0	0.358	1.000

The camera sensitivity was calibrated using astronomical sources (Venus). The measured B, G, and R band pixel brightness values for SRC and astronomical source are compared, and calibrated with the known magnitude of Venus, then translated into units of W / m^{-2} / nm using the zero point values to obtain the measured flux F_λ. This is translated into radiance by dividing by the solid angle subtended by the surface area of the SRC as seen from the observer $\Delta\Omega = 4\,\pi * A / D^2$ steradian, where A is the projected surface area (in m^2) and D the distance to the SRC (in m). The corresponding intensity: $I_\lambda = F_\lambda * (D^2 / 4\pi A)$. This radiance can be used to determine the surface brightness temperature if the emission is dominated by a blackbody continuum.

The radiance of a gray body is described by the Planck function (in this paper expressed in units of W cm^{-2} μm^{-1} $sterr^{-1}$):

$$B_\lambda (T) = 2\,h\,c^2 / \lambda^5 \quad * 1 / [\, exp\, (h\,c/\lambda\,k\,T) - 1]$$

multiplied by a wavelength-independent emissivity ε. This describes how much radiation energy is traveling through a differential surface δA at an angle θ to the normal of that area into a differential solid angle δΩ, per unit of time t and per unit of wavelength λ. In which case, with λ in units of nm:

$$T = 1.4388379 \times 10^7 / \lambda / (\, ln\, (1.0 + 1.191071 \times 10^{20}\, \varepsilon / (\lambda^5\, I_\lambda))\,)$$

. The projected surface area of the shield is A = 1.81 m^2 when viewed face-on ($\alpha = 0^o$) and smaller if the viewing angle α increases (Table I). The material emissivity ε for the Genesis heatshield (the ratio of the emitted intensity to the Planck function) is not known to us, but can be measured from the recovered shield. Literature values for various carbon materials give values ranging from 0.73 to 0.97. We adopt ε = 0.88, independent of wavelength (gray body).

Six still images of Venus were taken with the same camera at a shutter speed of 1/640 s and 300 mm focal length at altitude during the Sept. 07 Hyperseed MAC test flights. The disc of Venus was 19" in size, but was not resolved. Each image was slightly out of focus, the red fields more so than the blue fields. None of the image pixels were saturated. The planet's emission is reflected light from a G2V star, our Sun. Venus was at an elevation of 20 ± 3^o degree and had a brightness for the Johnson UVBRI filters: B = -3.52, V = -4.19, R = -4.51, I = -4.70 magnitudes (61% illuminated disk at phase angle 77^o, at a distance of 0.877 AU). The sky background was very homogeneous.

‡ Registered trademarks mentioned herein are the property of their respective owners.

Table II: Results of mean surface brightness temperatures *from R, G, B bands.*

Time:	D (km)	t(s)	Blue: T(K)	Green: T (K)	Red: T (K)
15:54:01	86.8	74.6	2134±8 *)	2030±11	1998±20
15:54:02	82.7	75.6	2106±8	2011±11	1988±17
15:54:03	79.0	76.6	2081±11	1994±10	1969±16
15:54:04	75.8	77.6	2051±14	1983±10	1969±18
15:54:05	73.1	78.6	1991±7	1928±12	1910±18
15:54:06	70.9	79.6	1968±12	1916±9	1908±17
15:54:07	69.1	80.6	1922±7	1897±9	1890±16
15:54:08	67.8	81.6	1906±15	1795±11	1759±14
15:54:09	66.9	82.6	1859±28	1766±8	1758±15
15:54:10	66.4	83.6	1851±23	1732±12	1766±22
15:54:11	66.2	84.6	1847±15	1709±10	1714±23

*) error includes only photometric uncertainty, no systematic errors from emissivity.

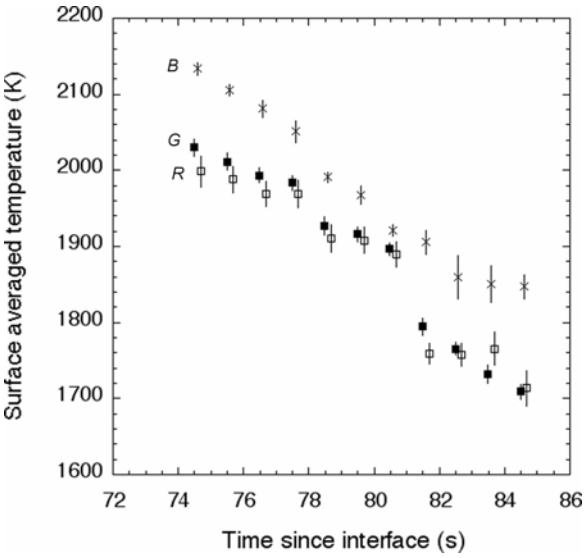

Figure 8. Brightness temperatures *derived from observed emission intensities in the blue, green and red bands. Time since passing the 135.0 km point.*

Each image consists of blue, green, and red filtered fields, each of which was calibrated separately. The relative intensities of the three bands were close to that expected from gray body emission. The corresponding temperatures are given in Table II and in Figure 8.

While the red and green fields are in excellent agreement, the blue images are systematically brighter than expected, and don't show the sudden decline at t = 81 seconds. The cause of this is probably the presence of N_2^+ band emission (Figure 4). If so, the higher-than-expected intensity of the blue field implies a contribution from molecular band emission up to 46% of the total emission in the B-band.

3. AIMIT camera: I-band brightness.

The Genesis SRC was detected briefly by the wide field acquisition camera of the "AIMIT" tracker (Astrobiology Instrument for Meteor Imaging and Tracking). The intent of this experiment was for the wide field acquisition camera to track the Genesis SRC bolide and direct the light into the slit of an Echelle spectrograph for high resolution spectroscopy at 300 – 900 nm.

Concerned about background sky brightness variations, we chose a manual acquisition of the object rather than an automatic acquisition as with meteors. Sadly, the object passed only through a corner of the field of view, too brief for an operator to put the cursor on the moving object. Nevertheless, the I-band detection can be used to measure the brightness temperature variation during peak heating.

The wide field acquisition camera was a low-light level KT&C™ "Hi-res EX Vision" black and white CCD Camera, 6 – 60 mm varifocal lens (f1.4) set at a fixed position, and equipped with a Scott RG 1000 long-pass cut-off filter (central wavelength of 863.7 nm, 0.001% transmission at 770 nm, 50% transmission at 1000 nm, 99% transmission above 1300 nm). The camera used the Sony EX-View CCD chip. The camera was positioned at 12.0 ± 0.1 ^{o} elevation, square (±1^{o}) to a 3/4" thick 12 inch diameter Quartz window (GE-105). The camera was fixed mounted and operated in a staring mode. The NTSC video output was recorded on analog Hi-8 Sony CCDTRV66-

NTSC camcorder at 29.97 frames/s, odd and even fields. No time mark was recorded, because of the intended purpose of this camera.

There are 47 unobstructed frames (1.57 seconds). The period of acquisition was determined from the presumed trajectory of the Genesis SRC and the known orientation of the aircraft and instrument relative to the aircraft frame. From this, the camera recorded a part of the trajectory following time t + 62.5±0.5 s, close to peak heating.

No calibration measurements were made to determine the sensitivity of this fixed camera during flight as our cosmic calibration source (Venus) was not detected in the test flights. This introduced an uncertainty in the absolute flux scale. Post-flight analysis at sea level included imaging of the star Betelgeuse (HD39801) at night, maintaining the same focal length and filter system. It is an M1-2 Ia-Iab type star with an effective surface temperature of 2,400 K (matching the anticipated surface temperature of Genesis). To determine changes in gain setting (factor 5.4), we did the same exercise with observations of the Moon in the daytime sky at nearly the same sky background.

The result is T = 2,225±19 K, with an uncertainty of ±19 K from the photometry alone, ±54 K from calibration to astronomical sources, but at least ±148 K if we include the uncertainty in the gain factor.

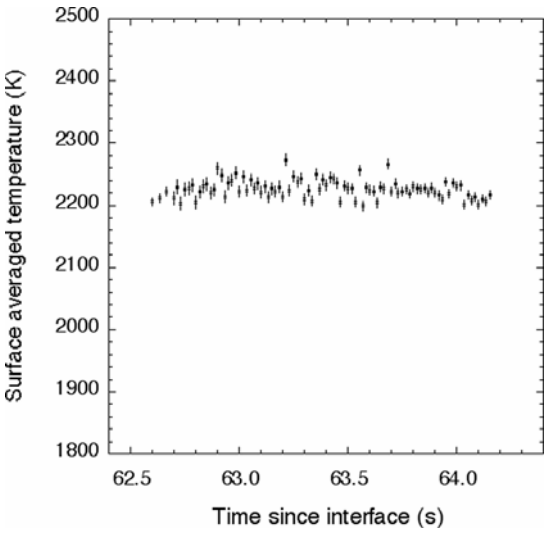

Figure 9. Results of I-band photometry, *after correction for instrument effects and for distance. Intensity in individual frames show that the SRC did not have large intensity variations.*

While the absolute calibration is uncertain, the signal-to-noise is high and this data is more suitable for addressing the potential variation of intensity on short time scales. The frame-to-frame brightness measurements were sufficiently accurate to search for rapid temporal variations in emission due to potential irregularities in the shock emission or capsule spin. As expected, we found no variations < 4% over time scales < 10 seconds (Figure 7). This is consistent with near-IR emissions being dominated by the surface gray body continuum emission (Fig. 4).

4. Ground-based video imaging.

Further photometric data was provided by a video record obtained with a hand-held camcorder from a ground-based location North West of Wells, Nevada. A Sony DCR-TRV510^{TM} camcorder operated by one of us (DH) recorded some 8 seconds of the SRC's trajectory on Digital Hi8 film. Purpose of this experiment was to document the Genesis SRC reentry and provide a record of visible brightness as a function of time. The camera (totally zoomed out in order not to loose the rapidly moving vehicle, was operated at f 1:1.4 3.6 mm. The focus was set to infinity. The weather was completely clear along the filmed part of the trajectory, with some clouds in the west.

The observers were located a few km northwest of Wells, Nevada at 41 degrees 8.604 minutes N (41.1434 N); 114 degrees 59.031 W (114.98385 W) (WGS 84), or 4,556, 435 N; 669,276 E (CONUS NAD27 datum) at approx. 5889 ft. altitude. The Sun was at 17º 52.319' elevation at 98º 38.39' azimuth. The Moon was bearing 76º 19.690' elevation at 170º 26.191'. A light wind was from northwest (~5km/hr). The ground temperature was 16.6 ºC.

The fireball was observed visually for approximately 15 seconds. Images of the SRC could be retrieved and were processed in their digital form from the original tapes. The SRC could be recognized from the moment of acquisition until it passed just above the Moon. After that, the object was seen from behind and lost in the sky glow. It was observed visually to redden.

There is one verbal time stamp several minutes prior to the event that defines the time to ±0.5 second. It puts the time of the SRC seen passing by the Moon at 15:53:46.0 ± 0.5 UT. This is 10 seconds earlier than predicted by the

SRC trajectory, which has the object pass the Moon at 15:53:56.2 UT as seen from the Wells site. We suspect an error in the time stamp and adopted the 15:53:56.2 time.

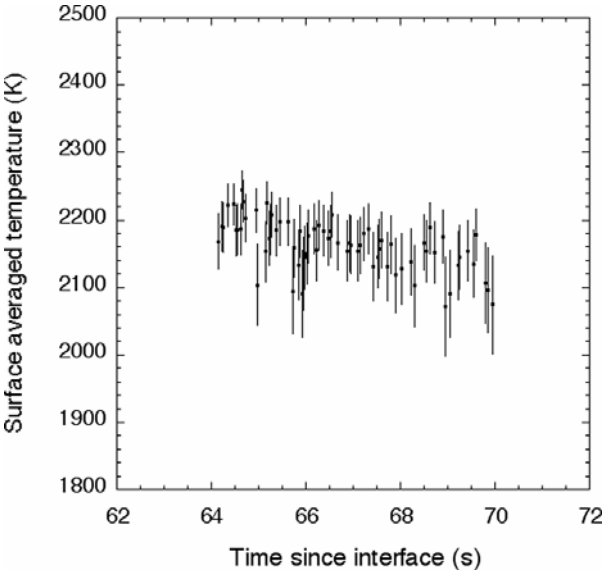

Figure 10. Surface-average brightness temperatures *derived for the green and red fields. Odd and Even fields are averaged.*

The quality of the images is much less than those discussed earlier. Each frame of 1/60s exposure consists of only 9-12 pixels on a bright background. The signal was not saturated, but varied significantly in brightness from one frame to the next, presumably due to motion blurring.

The SRC was marked by arrows in each frame, then decomposed in its R, G, and B frames, then split in odd and even fields. A background frame taken a short time earlier was subtracted and the sum of pixel intensity measured. The object was mostly just right of the center of the field of view, while it was followed on its path along the sky.

To calibrate the observed brightness, the Moon's images were processed in the same way as those of the SRC. The Moon's magnitudes in the Johnson bands were B = -8.43, V = –9.10, and R = -9.42 magn. at that time. The resulting photometry of the Moon has a 1 sigma standard deviation better (17%) for the green fields than for the blue and red fields (26%) because there are typically twice as many green pixels than there are blue or red pixels. There is no change in the Moon's brightness while it moves from the edge of the field to the center. Hence, no flatfielding correction is applied to the SRC observations. The blue band is most uncertain because of the high sky background.

The resulting brightness temperatures for the Green band (Fig. 10) are in good agreement with the airborne measurements (Fig. 6). The temperature shows a gradual decrease from a maximum at or before time 63.5 seconds. Again, we find that the blue band is more intense than expected. Median temperatures for the odd and even blue fields centered at 460 nm are: 2,395±14 and 2,421±11 K. This compares to 2,163±12 and 2,174±11 for the green field centered at 535 nm. The red field centered at 620 nm is slightly less intense than expected: 1,965±12 and 1,968±9 K, respectively. Some of the discrepancy may come on account of the spectral response curves of each field being very broad and overlapping.

5. Midwave infrared camera: 3.6 – 5.0 micron photometry.

In the same time interval as the AIMIT experiment on FISTA, at the time of peak heating, a nearly co-aligned mid-wave IR camera detected the Sample Return Capsule. This was an FSI^{TM} / Forward Looking Infrared Radiometer (FLIR) model Prism DS, with a Platinum Silicide focal plane detector array of 320 x 240 pixels with a field of view of 13 x 18 degrees. The images were recorded on NTSC video and are shown in multiple color palette, with a scale bar provided (Fig. 11). The camera was pointed at an elevation of 13^{o}, biased in forward pointing direction by ~ 5^{o}, behind a 12" diameter Germanium window (Fig. 12), and operated in staring mode. Other relevant information: the cooling method is Stirling Cycle. Detector refresh rate: 60 Hz. Dynamic range 8 bit. Emissivity Adjustment = 0.10 – 1.00 (set at ε = 1.00 for this data collect). The thermal sensitivity is said to be < 0.10 at 30 ºC, with a measurement accuracy of 2% or ±2 degrees ºC over the measurement range of –10 to 450 ºC.

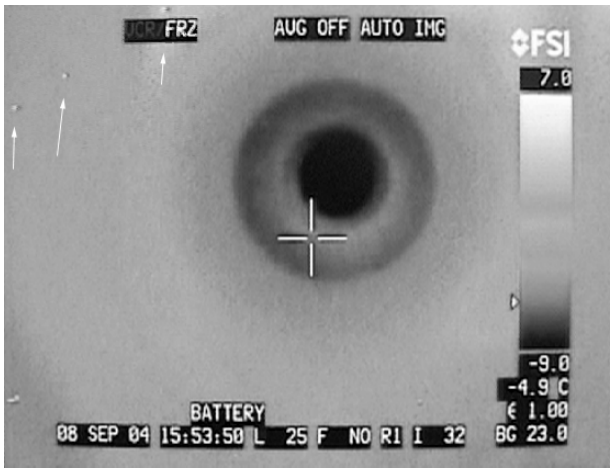

Figure 11. Example image *with superposed three detections of the SRC entry.*

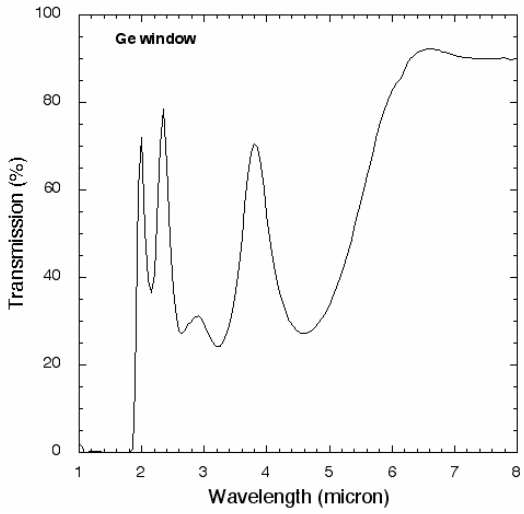

Figure 12. Window transmission *Germanium window.*

Four seconds of the Genesis SRC trajectory were recorded (15:53:48 to 15:53:52 UT, according to the camera internal clock, accurate to ±0.3 s, or from t = 61.6s to 65.6 s), during which time the object moved along a trajectory that cuts the top left corner of the field of view from left to right (arrows Figure 11). The distance to the SRC decreased from 197 km to 150 km. The location in the field and the part of the trajectory recorded cover that of AIMIT.

The images provide a measure of temperature indicated by a color scale that runs from –9.0 to +7.0 ºC. The signal of the SRC + background does not saturate and registers at a peak temperature of +3.2 -> +3.8 -> +4.5 ºC. The automatic scale (outer range is provided) is not changed when the SRC enters the field of view. The background brightness is a sum of sky brightness, emission from the window, and reflected light from the camera and cabin and at the level of ~ -1.3ºC.

The Aerospace Corporation mid-IR team undertook a calibration verification of these data. Results of the analysis were published by Rossano and Russell.[12] The temperature of a source pixel was measured relative to a background pixel and converted to an in-band flux at the entrance to the lens. This can be done to an equivalent precision of about 0.2 ºC (±2 K at 2,200 K). The absolute calibration of the camera introduced the largest uncertainty. The camera takes an emissivity * a Planckian black body flux and chooses the temperature that makes the calculated in-band radiance agree with the measured radiance. The manufacturer claims a temperature calibration of +/- 2 ºC over the range -10 C to 250 ºC, which was verified over the range of approx. 25 ºC to 200 ºC for sources that fill a pixel. The manufacturer claims a wavelength response from 3.6 to 5 μm. We verified this bandpass.

We believe the camera assigns temperatures by assuming the source fills a pixel and takes into account the overall response of the camera over a bandpass of 3.6 to 5 microns, with an emissivity of 1.0. The flux at the entrance to the lens would thus be obtained by integrating the Black Body function over 3.6 to 5 μm and applying the pixel solid angle of $\Delta\Omega = 1x\ 10^{-5}$ str. We assume that the camera does not correct for atmospheric absorption.

The approach to exploit the data would be to take the nearby background temperature and convert it to flux. Then do the same for the source pixel and subtract them. This residual is the flux from the source at the entrance to the lens. This would then be corrected for transmission of the atmosphere and the Germanium window to get the flux at the source in the 3.6 to 5 μm bandpass.

The following information and assumptions were used: The Germanium window had an average transmission of 0.7. The average transmission of the atmosphere was 0.95. The distance to the source was 190 km. The emissivity of the source was taken as 0.88. The projected area of the source was 1.7 m^2. With these values, a source temperature of

2,200±100 K was derived, in good agreement with results from emissions at optical wavelength. Hence, this mid-IR measurement is consistent with most of the emission deriving from a gray body continuum.

6. High speed photometer

Purpose of this experiment was to measure rapid photometric variations in the Genesis SRC reentry emission. Two radiometers were setup on FISTA in parallel, pointed 37° above the horizon, and measured the sky over a large +/- 15º field of view. A 10-nm wide 870 nm interference filter was used with one radiometer and a similar 656 nm filter was used with the other. The system was run for 90s at a rate of 250,000 samples per second, with Genesis in the FOV from t = 45 to 74s (since passing the 135 km altitude point). At about t = 65 seconds, the SRC brightness peaked and the spacecraft passed through the center of our field of view. Fast Fourier Transforms were obtained of the traces. These results did not show anything from the Genesis passing through the FOV, except perhaps a power increase at the spin frequency of the Genesis. We conclude that the fainter than expected luminosity from the sample return capsule was overwhelmed by the variations of sky brightness due to aircraft motion.

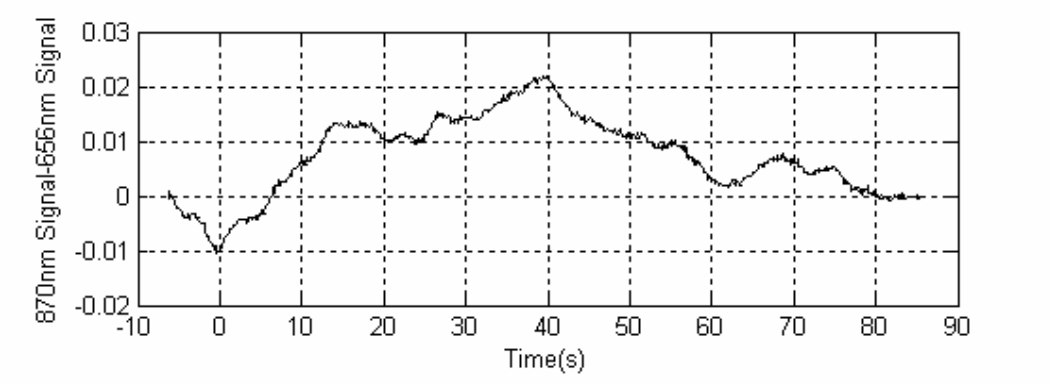

Figure 13. Normalized difference *between the two radiometer signals (time since passing 135 km), in units of* 10^{-8} W/cm^2.

The total combined filter-lens-detector responses were 0.18A/W/cm^2 for the 870 nm assembly and 0.11 A/W/cm^2 for the 656 nm assembly. There was some unfiltered light leakage around the edge of the filter. The amount of leakage was approximated by conducting an additional test in which a known area of the filter (0, 0.5, and 1in^2) was blocked and the intensity of clear-sky light (similar to that observed on the day of the reentry) was measured. The result was a 40% increase in the intensity of the signal.

The radiometer readout electronics contains DC background removal circuitry. At t = 0 the background removal circuit was switched off and held at its current state in an attempt to improve the acquisition of the slow-rising signal. Switching off the background removal circuit did come at the expense of allowing a slow, linear drifting of the output signals. This drift was removed from the signals prior to creating the plot in Figure 13.

The signals from the individual channels vary in unison because of changes in the pointing of the photometers from roll in the aircraft motion. Each signal is the sum of sky plus SRC. Figure 13 shows the difference between the signals acquired from the two radiometers. Prior to creating the difference plot, the signals were normalized; the signals were scaled to match the amplitudes using a signal swing present in both of the signals prior to when the reentry was known to have occurred (i.e. the 656 nm signal was scaled to make the amplitude of the large background signal swing centered at 30 seconds equal to the amplitude of the same swing in the 870 nm signal). The minimum and maximum bounds on the ratio can be approximated to 1.05 (+ 10% / - 15%). Note that these differences are at the level of 1-3% of the measured signals. The normalization affects the zero level, actual differences being of order 0.2 x 10^{-8} W/cm^2. The total expected signal from the SRC was about 0.006 x 10^{-8} W/cm^2, but the measured brightness suggests <0.002 x 10^{-8} W/cm^2, too faint to be detected.

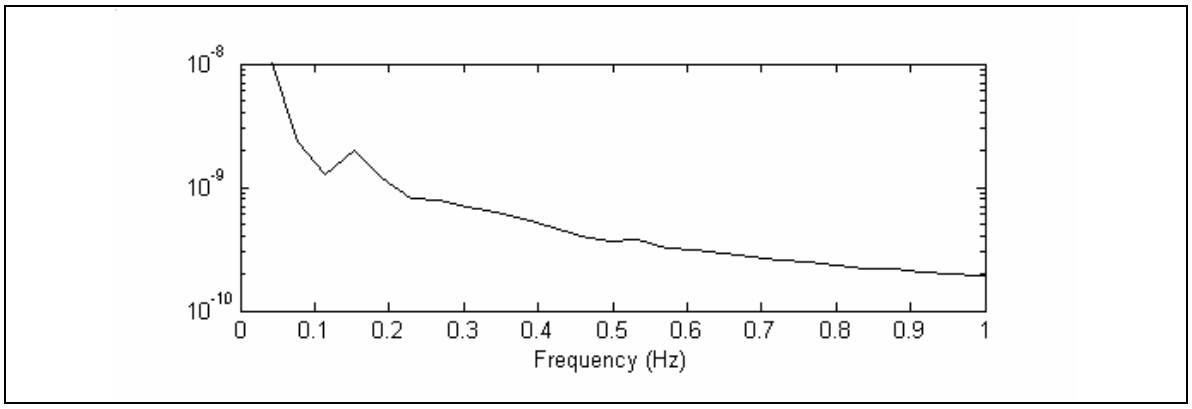

Figure 14. FFT of the 870nm signal *(time period from 60 to 84 seconds).*

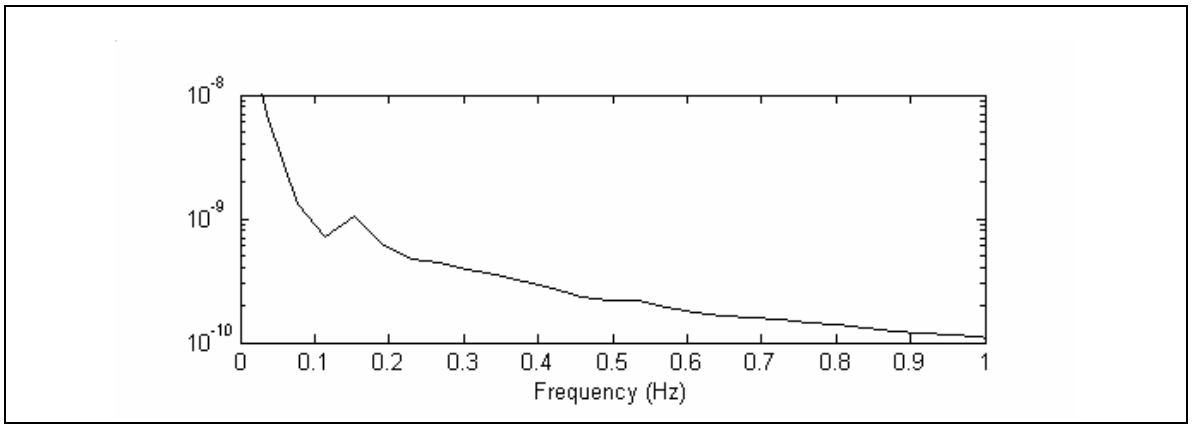

Figure 15. FFT of the 656nm signal *(time period from 60 to 84 seconds).*

A frequency-domain analysis was conducted by filtering as well as inspecting the FFTs of the signals in the relevant time domain between 60 and 84 seconds. The FFTs of the signals are shown below in Figures 15 and 16. The signals were filtered using many different bandpass filters that spanned the entire 0-125 kHz frequency band. The filtering analysis did not reveal any significant features in the time-domain signal that might be attributable to a detection of the event by the radiometers. The filtering was also used to inspect the data for the presence of any short transients. All of the short transients found in the data were linked to the hardware and determined not to be the result of events detected by the radiometer.

During the period of interest between t = 60 and 80 seconds, there may be excess power at 0.15 ± 0.03 Hz (6.67s) and perhaps around 0.53 Hz. The first value, 0.15 Hz, corresponds to a spin rate of 9.0 ± 1.8 cycles/minute, or twice the spinning rate of the Genesis SRC (16 cycles/minute). The second value is at half the SRC spinning rate. If this signal is real, there are a number of potential causes.

The fluctuations discussed above may have been due to aircraft attitude deviations, natural behavior of the atmosphere, or both. Either way, their amplitudes were orders of magnitude larger than that predicted for the signal of interest. The SRC signal is a small fraction of the total sky signal, making frequency-based signal separation approaches ineffective. We conclude that fluctuations in sky background intensity, and the disappointing brightness of the SRC, were such as to make attempts at extracting photometry of the reentering body futile.

8. Infrasound.

The infrasound of the sample return capsule reentry was loud enough to be recorded on camcorders on the ground. A three-channel detection was made with an infrasound array at Wendover airport. Results have been published elsehwere.[13] We conclude that the Genesis SRC Entry did not generate acoustic signals other than from its hypersonic shock wave, and this is consistent with the fact that the vehicle did not break up on re-entry (which would have generated multiple acoustic signals). The infrasound wavetrain amplitude (peak to peak) of 7.5 Pa (corrected for the instrument frequency response, etc.) is higher than the predicted 1 - 5 Pa, based on earlier NASA Apollo reentry data from various NASA reports, scaled for the size of Genesis compared to a much larger Apollo command module. The difference, however, can result from a different ground-penetration factor (~ 2) than used in the prediction (1.0). The wavetrain duration was in excess of 2 minutes, with energy recorded over a large range of altitudes and directions. We detected reflections from nearby mountain ranges. The dominant infrasound frequency spectrum peaked at 3 Hz. It was predicted to peak in the 1-10 Hz range.

Discussion and Conclusions

The observed optical emissions are consistent with the prediction that most of the emitted light is from a gray body continuum only. The same brightness temperature was derived for blue, green, red, near-infrared and mid-infrared wavelengths, covering the range 400 - 5,500 nm. There were no significant (> 4%) variations in light intensity over short (< 10 s) time scales during peak heating. High-speed (250,000 samples/s) photometric observations did not show brief intensity fluctuations strong enough to be detected over the sky background.

Some variation of relative band intensity in the final part of the trajectory leaves open the possibility of contributing emissions from other than a gray body continuum. The blue band intensity was higher than expected for a blackbody curve, consistent with the predicted relative presence of N_2^+ band emission compared to blackbody emission at the lower surface temperatures measured.

The peak surface temperature of 2,200±50 K is less than the ~ 2,630 K surface-averaged temperature derived from our models. In early parts of the trajectory, the surface was as much as 570 K cooler than predicted, and the SRC was about 2.5 magnitudes fainter correspondingly. After peak heating, the surface cooled less rapidly than expected.

Based on ground and flight test data at relevant conditions, it is expected that the incident heat flux at these conditions can be calculated to within 20%, which is much better than the discrepancy in surface temperature as reported. Therefore, the problem must be in computing the NET heat flux, that is the portion re-radiated away.

The blackbody surface temperature estimates were made from fully catalytic radiative equilibrium CFD calculations, which can be too high for several reasons:

(1) conduction into the material, which accounts for a non-trivial portion of the total incident heat flux,

(2) ablation/pyrolysis products, which carry heat away from the surface and have a significant cooling effect,

(3) and finite-rate wall catalycity, which could lower the heating rates below the fully catalytic predictions.

Of these, the first two should be the most important; the surface, being made of carbon, should be highly catalytic. The high-density high-temperature (2,870 K) deposited carbon-carbon sheet is thermally conductive and the underlying low-density carbon foam insulator acts as a heat sink.

Future work

Further scrutiny is warranted to verify the Genesis SRC data. We aim to apply the lessons learned to observations of the Stardust Sample Return Capsule reentry on January 15, 2006. This is a faster reentry, from which much stronger shock emissions can be expected and a significant amount of radiative heating. The Stardust SRC also has an ablative heat shield, which makes the remote sensing of radiative signatures from ablation products more likely. These hypervelocity entry trajectories are better known hours before entry than estimated by entry dispersion

analysis at much earlier times.[14] And because Stardust will return at night, around 2 a.m. PST (local time in Nevada) in the morning, we will not need the restrictive fields of view for the acquisition cameras.

Confirmation of the lower-than-expected surface temperature would validate the Genesis results and provided further guidance to improving future engineering models for TPS design.

Acknowledgments

The Genesis SRC Entry observing campaign was sponsored by the NASA Engineering and Safety Council. The mission was executed by the USAF 412th Test Wing at Edwards Air Force Base. NASA Ames Research Center and the SETI Institute coordinated the mission. At NASA Ames, management support was provided by Chuck Smith, Günter Riegler, and Center director Scott Hubbard. The calibration validation of the midwave camera was supported at The Aerospace Corporation by the Center for Orbital and Reentry Debris Studies, Dr. W. Ailor, Director.

References

[1]Desai, P. N., Mitcheltree, R. A., and Cheatwood, F. M., 2000. Sample return missions in the coming decade. 51st International Astronautical Conference, 2-6 Oct. 2000, Rio de Janeiro, Brazil, IAF-00-Q.2.04.

[2]Olynick D., Chen, Y.-K., and Tauber, M. E., 1999. Aerothermodynamics of the Stardust Sample Return Capsule. J. Spacecraft and Rockets **36**, 422-462.

[3]Jenniskens, P., Wilson, M. A., Packan, D., Laux, C. O., Krueger, C. H., Boyd, I. D., Popova, O. P., and Fonda, M., 2000a. Meteors: A delivery mechanism of organic matter to the early Earth. *Earth, Moon and Planets* **82-83**, 57-70.

[4]Jenniskens, P., Wercinski, P., Olejniczak, J., Allen, G., Desai, P. N., Raiche, G., Kontinos, D., Revelle, D., Hatton, J., Baker, R. L., Russell, R. W., Taylor, M., and Rietmeijer, F., 2005. Preparing For Hyperseed MAC: An Observing Campaign To Monitor The Entry Of The Genesis Sample Return Capsule. Earth, Moon and Planets (DOI: 10.1007/s11038-005-9021-2).

[5]Tran, H., Johnson, C., Rasky, D., Hui, F., Chen, Y. K., and Hus, M., 1996. Phenolic impregnated carbon ablators (PICA) for Discovery Class missions. AIAA Paper No. 96-1911.

[6]Marrone, P. V., and Wurster, W. H., 1970. Reentry precursor plasma – determination of the vacuum ultraviolet photoionizing radiation flux, *The Entry Plasma Sheath and its Effects on Space Vehicle Electromagnetic Systems*, Vol. 1. NASA SP-252.

[7]Presley, L. R., and Omura, M., 1970. Microwave measurement of precursor electron densities ahead of shock waves in air at velocities greater than 10 km/s", AIAA Paper 70-83.

[8]Lin S.-C., 1962. Radio echoes from a manned satellite during re-entry. *J. Geophys. Res.* **67**, 1962, 3851-3869.

[9]Jenniskens, P., Butow, S. J., and Fonda, M., 2000b. The 1999 Leonid Multi-Instrument Aircraft Campaign - an early review. *Earth, Moon and Planets* **82-83**, 1-26.

[10] Swift W., and Suggs R., 2006. Genesis Reentry Observations and Data Analysis. NASA/TM-2005-214192, published by Marshal Space Flight Center.

[11]Biu, C. (2004) "Spectroscopy, CCD & Astronomy" web site.

[12]Rossano, G. S., and Russell R. W., 2005. Use of a FLIR-Midwave Camera During the Genesis Recovery Mission. AEROSSPACE REPORT No. ATR-2005(9368)-1. The Aerospace Corporation, El Segundo, California.

[13] Revell, D. O., Edwards, W., Sandoval, T. D., 2005. Genesis--An artificial, low velocity "meteor" fall and recovery: September 8, 2004. *Meteoritics & Planetary Science* **40**, p.895.

[14]Desai, P. N., and Cheatwood F. M., 1999. Entry dispersion analysis of the Genesis Sample Return Capsule. AAS/AIAA Astrodynamics Specialist Conference, Girdwood, Alaska, AAS Paper No. 99-469.